Simulations of the effects of density and temperature profile on SMBI penetration depth based on the HL-2A tokamak configuration*

Xueke Wu(吴雪科)[1], Huidong Li(李会东)[1,†], Zhanhui Wang(王占辉)[2,‡], Hao Feng(冯灏)[1], and Yulin Zhou(周雨林)[2]

[1] School of Science, Xihua University, Chengdu 610039, China
[2] Southwestern Institute of Physics, Chengdu 610041, China

(Received 5 November 2016; revised manuscript received 13 March 2017; published online 20 April 2017)

Using the *trans-neut* module of the BOUT++ code, we study how the fueling penetration depth of supersonic molecular beam injection (SMBI) is affected by plasma density and temperature profiles. The plasma densities and temperatures in L-mode are initialized to be a set of linear profiles with different core plasma densities and temperatures. The plasma profiles are relaxed to a set of steady states with different core plasma densities or temperatures. For a fixed gradient, the steady profiles are characterized by the core plasma density and temperature. The SMBI is investigated based on the final steady profiles with different core plasma densities or temperatures. The simulated results suggest that the SMB injection will be blocked by dense core plasma and high-temperature plasma. Once the core plasma density is set to be $N_{i0} = 1.4N_0$ ($N_0 = 1 \times 10^{19}$ m^{-3}) it produces a deeper penetration depth. When N_{i0} is increased from $1.4N_0$ to $3.9N_0$ at intervals of $0.8N_0$, keeping a constant core temperature of $T_{e0} = 725$ eV at the radial position of $\psi = 0.65$, the penetration depth gradually decreases. Meanwhile, when the density is fixed at $N_{i0} = 1.4N_0$ and the core plasma temperature T_{e0} is set to 365 eV, the penetration depth increases. The penetration depth decreases as T_{e0} is increased from 365 eV to 2759 eV. Sufficiently large N_{i0} or T_{e0} causes most of the injected molecules to stay in the scrape-off-layer (SOL) region, lowering the fueling efficiency.

Keywords: tokamak, plasma fueling, SMBI, penetration depth, HL-2A

PACS: 52.25.Fi, 52.25.Ya **DOI:** 10.1088/1674-1056/26/6/065201

1. Introduction

To achieve the high-confinement mode in most magnetic fusion machines, such as the ITER tokamak, it is necessary to improve the fueling efficiency and fueling penetration depth. Three main methods have been used to fuel tokamak machines: gas puffing (GP),[1] pellet injection (PI),[2] and supersonic molecular beam injection (SMBI).[3] In gas puffing, its penetration depth is very shallow and its fueling efficiency is very low. Most of the puffed molecules remain outside of the last-closed flux surface during GP, and the molecules penetrate into the plasma injected mainly through thermal diffusion (i.e, local T_e cooled). Although pellet injection (PI) has a deep penetration depth and high fueling efficiency, it is expensive. Therefore, it is desirable to find a new fueling method with high efficiency but low cost. Supersonic molecular beam injection (SMBI) is an improvement on GP with a radial directed supersonic group velocity generated by a special designed Laval nozzle. In SMBI, the injected molecules interact with the fusion plasma directly, which differs from PI with the stripping (ablation) and shielding process. Different from GP, whose fueling process is dominated by diffusion, convection plays a key role in SMBI owing to the high directed group velocity of the SMB. Experiments have proven that SMBI has higher fueling efficiency and deeper injection than GP. Although PI has a high penetration depth, it costs more than SMBI.

SMBI is not only a fueling method but also an efficient way to control plasma behavior. It can control the plasma density,[4] trigger the L–H transition and improve confinement,[5] and simultaneously control and mitigate the edge-localized mode (ELM).[6] Even more, it can be used to experimentally investigate non-local heat transport,[7] impurity transport,[8] and particle transport.[9] Considering all of these advantages of SMBI, we believe that the fueling problems about the penetration depth of SMBI must be studied.

To improve the fueling performance of SMBI, some experimental investigations[3,4,10] have been performed to improve its penetration depth and fueling efficiency, such as by converting from low (magnetic) field side injection to high (magnetic) field side injection, changing the SMB speed, tem-

*Project supported by the National Natural Science Foundation for Young Scientists of China (Grant No. 11605143), the Undergraduate Training Programs for Innovation and Entrepreneurship of Sichuan Province, China (Grant No. 05020732), the National Natural Science Foundation of China (Grant No. 11575055), the Fund from the Department of Education in Sichuan Province of China (Grant No. 15ZB0129), the China National Magnetic Confinement Fusion Science Program (Grant No. 2013GB107001), the National ITER Program of China (Contract No. 2014GB113000), and the Funds of the Youth Innovation Team of Science and Technology in Sichuan Province of China (Grant No. 2014TD0023).

†Corresponding author. E-mail: huidongli888@163.com
‡Corresponding author. E-mail: zhwang@swip.ac.cn

© 2017 Chinese Physical Society and IOP Publishing Ltd

perature, and particle flux intensity, as well as the background electron density and temperature. The effects of plasma density and temperature on penetration depth can be researched experimentally by using methods such as fast TV cameras and charge-exchange recombination spectroscopy.[11,12] However, such experimental methods are limited in their abilities to directly measure the penetration front of neutral particles, particle transport, and various collision reactions. Some simulations have been performed in order to improve the penetration depth, such as by comparing GP and SMBI[13] and by studying the effect of SMBI flux.[14]

Large-scale real-time numerical simulations can provide detailed temporal–spatial information on neutral front propagation and collision reactions, because such simulations are not constrained by the complicated technical problems present in experiments. There exist some codes for performing this kind of simulation, such as B2,[15] EPIC,[16] UEDGE,[17,18] BOUT/BOUT++,[19–21] and TOKES.[22] The BOUT++ code is used to study edge plasma physics, with its physical transport models based on two fluid MHD equations. The BOUT++ code is a software platform for simulating two-dimensional (2D) and three-dimensional (3D) fluid plasma in an arbitrary curvilinear coordinate system. With the BOUT++ framework, many practical subroutine modules have been developed, such as the *trans-neut*[23] module, which issued for studying macroscopic transport dynamics in 3D simulations, and the TPSMBI code,[24] used for studying the radial transport dynamics of SMBI. Performing a 3D spatial–temporal simulation of the real tokamak geometry with X-point would require massive CPU time and number of tasks that need to be submitted, then this paper simply assumes toroidal symmetry for some basic studies, such as radial propagation of neutral particles, because the toroidal asymmetry makes little difference to the radial propagation of neutral particles. Therefore, 2D simulation via *trans-neut* is applied to study the fueling problems of SMBI. The simulation considers four kinds of main collision reactions: those among hydrogen molecules, atoms, electrons, and ions. It also accounts for particle recycling, the sheath effect, and the local constant flux boundary condition.

In the present paper, we will use the *trans-neut* module of the BOUT++ code to study how the background plasma affects SMBI penetration in the HL-2A tokamak. In order to understand how the plasma density and the temperature profiles affect the SMBI penetration depth and fueling efficiency, we will perform simulations through the developed *trans-neut* module. Section 2 introduces the physical model. Section 3 gives the boundary conditions of the numerical calculations. Section 4 illustrates the simulated results. Finally, Section 5 summarizes the principal results.

2. Physical model

It is to study the fueling physics of SMBI by using the MHD equations. Tokamak plasma contains multiple species, including hydrogen molecules, atoms, ions, and electrons. Thus, the SMBI fueling problem in HL-2A tokamak plasmas relates to sophisticated physical processes. Considering the difficulties in the calculation and simulation, four main kinds of collision reactions between various species are considered during SMBI: the molecular dissociation reaction (molecular-dissociated reaction), the atom-ionizing reaction, the charge-exchange reaction between atoms and ions, and the recombination reaction between electrons and ions. Our physical model considers some primary physical effects, including perpendicular plasma density diffusion, atom diffusion, heat diffusion and conduction, parallel plasma density convection, molecule radial density convection, energy interchange between ions and electrons, and parallel ion viscosity. This model uses the seven-field model deduced from the Braginskii equations, and it solves for the molecule and atom density, ion and electron temperatures, parallel plasma velocity, and molecule radial velocity. The transport equations of the model are given as follows:[25]

$$\frac{\partial N_{\rm i}}{\partial t}+\nabla_{\parallel}\left(V_{\parallel{\rm i}}N_{\rm i}\right)-D^{\rm c}_{\perp{\rm i}}\nabla^2_{\perp}N_{\rm i}=S^{\rm p}_{\rm I}-S^{\rm p}_{\rm rec}, \tag{1}$$

$$\begin{aligned}&\frac{\partial T_{\rm i}}{\partial t}+V_{\parallel{\rm i}}\nabla_{\parallel}\left(T_{\rm i}\right)+\frac{2}{3}T_{\rm i}\nabla_{\parallel}V_{\parallel{\rm i}}\\&-\frac{2}{3N_{\rm i}}\nabla_{\parallel}\left(\kappa^{\rm c}_{\parallel{\rm i}}\nabla_{\parallel}T_{\rm i}\right)-\frac{2}{3}\chi^{\rm c}_{\perp{\rm i}}\nabla^2_{\perp}T_{\rm i}\\=&\left(\nu_{\rm rec}-\nu_{\rm I}\right)T_{\rm i}+\frac{2m_{\rm e}}{M_{\rm i}}\frac{T_{\rm e}-T_{\rm i}}{\tau_{\rm e}},\end{aligned} \tag{2}$$

$$\begin{aligned}&\frac{\partial V_{\parallel{\rm i}}}{\partial t}+V_{\parallel{\rm i}}\nabla_{\parallel}V_{\parallel{\rm i}}-\frac{4}{3N_{\rm i}M_{\rm i}}\nabla_{\parallel}\left(\eta^0_{\rm i}\nabla_{\parallel}V_{\parallel{\rm i}}\right)\\=&-\frac{\nabla_{\parallel}P}{N_{\rm i}M_{\rm i}}-\left(\nu_{CX}+\nu_{\rm I}\right)V_{\parallel{\rm i}},\end{aligned} \tag{3}$$

$$\begin{aligned}&\frac{\partial T_{\rm e}}{\partial t}-\frac{2}{3N_{\rm i}}\nabla_{\parallel}\left(\kappa^{\rm c}_{\parallel{\rm e}}\nabla_{\parallel}T_{\rm e}\right)-\frac{2}{3}\chi^{\rm c}_{\perp{\rm e}}\nabla^2_{\perp}T_{\rm e}\\=&\nu_{\rm rec}W_{\rm rec}-\nu_{\rm I}\left(T_{\rm e}+\frac{2}{3}W_{\rm I}\right)\\&-\frac{2}{3}\nu_{\rm diss}\left(W_{\rm diss}+W_{\rm bind}\right)-\frac{2m_{\rm e}}{M_{\rm i}}\frac{T_{\rm e}-T_{\rm i}}{\tau_{\rm e}},\end{aligned} \tag{4}$$

$$\begin{aligned}&\frac{\partial N_{\rm a}}{\partial t}-\nabla_{\parallel}\left(D^{\rm c}_{\parallel{\rm a}}\nabla_{\parallel}N_{\rm a}\right)-D^{\rm c}_{\perp{\rm a}}\nabla^2_{\perp}N_{\rm a}\\=&-S^{\rm p}_{\rm I}+S^{\rm p}_{\rm rec}+2S^{\rm p}_{\rm diss},\end{aligned} \tag{5}$$

$$\frac{\partial N_{\rm m}}{\partial t}+\nabla_x\left(V_{x{\rm m}}N_{\rm m}\right)=-S^{\rm p}_{\rm diss}, \tag{6}$$

$$\frac{\partial V_{x{\rm m}}}{\partial t}+V_{x{\rm m}}\nabla_x V_{x{\rm m}}=-\frac{\nabla_x P_{\rm m}}{N_{\rm m}M_{\rm m}}. \tag{7}$$

Plasma transport is described in Eqs. (1)–(4), which use the quasi-neutral condition ($N_{\rm i}=N_{\rm e}$). Atom transport is given in Eq. (5), and molecule transport is included in Eqs. (6) and (7), where the molecule pressure is, T_m is the molecule temperature (usually room temperature), and k is

Boltzmann's constant. Our simulation uses field-aligned coordinates (x, y, z), which can be transformed into the common orthogonal toroidal coordinate (ψ, θ, ξ) via coordinate conversion.[19–21]

In this simple model, all source and sink terms of particle and heat are due to atomic and molecular reactions, such as molecules dissociation, atoms ionization, ion–atom charge exchange, and electron–ion recombination. The interactions between atom, molecule and plasma are included self-consistently. This model captures some basic transport physics during SMBI on both perpendicular and parallel directions, including: i) with a constant injection flux of molecule density at the outermost boundary flux surface, neutral molecules and atoms propagate inwards continuously due to molecule convection and atom diffusion effect; ii) both locally peaked plasma density and locally decreased plasma temperature profiles are formed due to both particle fueling and heat sinking effects of SMBI via neutrals dissociation and ionization, even though there is strong parallel convection and conduction transport; iii) the locally peaked plasma density will dramatically increase the losing rates of molecule and atom which prevents the further penetration of SMBI; iv) propagating front of molecules stagnates due to the total molecule dissociation rate balancing with the molecule injection rate at the SMBI source; v) plasma density blobs (i.e., source) and ion temperature holes (i.e., sink) propagate on the parallel direction due to parallel convection effects.

3. Boundary conditions

Our simulation uses the real magnetic geometry of the HL-2A tokamak with X-point (Fig. 1). This geometry can be divided into three solving regions: the plasma core and edge region, the scrape-off-layer (SOL) region, and the private flux and divertor plate region. In the simulation, different boundary conditions are set in each solving region.

Neumann radial boundary conditions are set for all evolving quantities, such as for N_m, N_a, $V_{x\mathrm{m}}$, and V_i, except for N_i, T_i, and T_e at the innermost boundary flux surface of the core side. For N_i, T_i, and T_e, the fixed-gradient or flux-driven boundary conditions are given as follows:

$$\left.\frac{\partial N_\mathrm{i}}{\partial x}\right|_{\mathrm{core}} = -C_{\mathrm{Ni}}\frac{N_0}{L_0^2 B_0}, \tag{8}$$

$$\left.\frac{\partial T_{\mathrm{e,i}}}{\partial x}\right|_{\mathrm{core}} = -C_{\mathrm{Te,i}}\frac{NT_0}{L_0^2 B_0}, \tag{9}$$

where the normalized parameters are set to $L_0 = 2.07$ m (the largest radius of the HL-2A tokamak), $N_0 = 1.0\times10^{19}$ m^{-3} (the characteristic plasma density at the core), $T_0 = 10$ eV (a reference temperature at the edge) and $B_0 = 1.96$ T (the magnetic field on axis). To study how the plasma density affects the SMBI in this simulation, the coefficient $C_{\mathrm{Te,i}}$ is set constant at $C_{\mathrm{Te,i}} = 25100$, but the parameter C_{Ni} characterizing the core plasma density gradient is set to be a series of values from 200 to 1400 at intervals of 300. Steady states of the five initial plasma density profiles characterized by C_{Ni} are achieved by *trans-neut*. The SMBI with a pulse duration of 1.0 ms is turned on, based on the obtained steady states in our simulations.

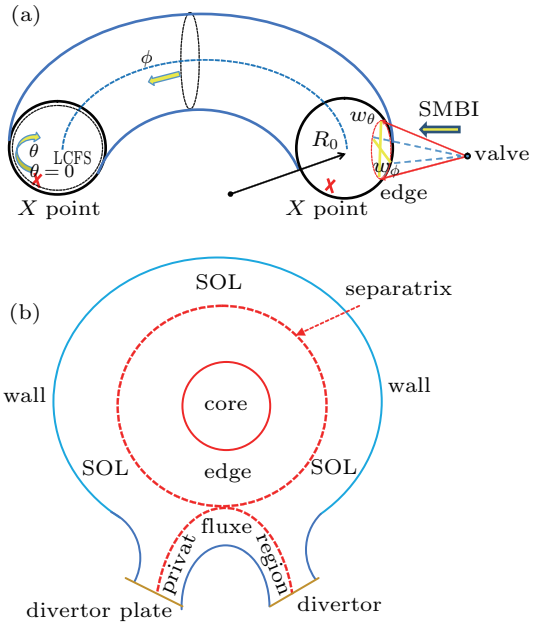


Fig. 1. (color online) SMBI configuration of HL-2A (a) and the different solving regions on the poloidal cross-section of HL-2A (b).

We also investigate how the plasma temperature affects the fueling of SMBI. For this case, the plasma density gradient is set constant as 500, while the electron and ion temperature gradient is set to 12550, 25100, 50200, 75300, or 100400. Also, the plasma first evolves into five steady states for each set of $(C_{\mathrm{Ni}}, C_{\mathrm{Te,i}})$. Then the same SMBI is turned on in order to study the SMB penetration depth at various initial temperature profiles.

On the innermost magnetic surface of the private flux region, the following Dirichlet boundary conditions are applied: $N_\mathrm{i}|_{\mathrm{pf}} = 0.1N_0$ and $T_\mathrm{e}|_{\mathrm{pf}} = T_\mathrm{i}|_{\mathrm{pf}} = T_0$. At the outermost flux surface in the SOL and private flux regions, Neumann boundary conditions are also used for all evolving quantities except N_i, T_i, T_e, and N_a. The Dirichlet boundary conditions are used for T_i and T_e, the same as in the private flux region. While the particle recycling boundary conditions are applied to N_i and N_a, as shown below:

$$\left.\frac{\partial \ln(N_\mathrm{i})}{\partial x}\right|_{\mathrm{wall}} = -\frac{1}{\sqrt{g^{11}}L_{\mathrm{Ni}}^{\mathrm{w}}}, \tag{10}$$

$$\left.\frac{\partial \ln(N_\mathrm{a})}{\partial x}\right|_{\mathrm{wall}} = \frac{\Gamma_\mathrm{a}^{\mathrm{w}}}{\sqrt{g^{11}}D_{\perp\mathrm{a}}^{\mathrm{c}}}, \tag{11}$$

where the plasma density gradient length at the wall $L_{\mathrm{Ni}}^{\mathrm{w}} = 5$ cm is an input parameter, the recycling neutral atom flux from the wall to the plasma is calculated by $\Gamma_\mathrm{a}^{\mathrm{w}} = R_{\mathrm{cyc}}\Gamma_\mathrm{i}^{\mathrm{w}} =$

$R_{\rm cyc}D^{\rm c}_{\perp{\rm i}}N_{\rm i}/L^{\rm w}_{\rm Ni}$, and the particle recycling rate is set to $R_{\rm cyc}=1.0$.

On the divertors, the sheath boundary conditions (12)–(14) and the particle-recycling boundary conditions (15) are used, as shown below:

$$V_{\|{\rm i}}|_{\theta=0}=-c_{\rm se}|_{\theta=0};\quad V_{\|{\rm i}}|_{\theta=2\pi}=c_{\rm se}|_{\theta=2\pi}, \tag{12}$$

$$\nabla_{\|}N_{\rm i}|_{\theta=0}=0;\nabla_{\|}N_{\rm i}|_{\theta=2\pi}=0, \tag{13}$$

$$\nabla_{\|}T_{\rm e,i}|_{\theta=0}=Q^{\rm d}_{\rm e,i}/(k\kappa^{\rm c}_{\|{\rm e,i}})|_{\theta=0},$$

$$\nabla_{\|}T_{\rm e,i}|_{\theta=2\pi}=-Q^{\rm d}_{\rm e,i}/(k\kappa^{\rm c}_{\|{\rm e,i}})|_{\theta=2\pi}, \tag{14}$$

$$\nabla_{\|}N_{\rm a}|_{\theta=0}=-\Gamma^{\rm d}_{\rm a}/D^{\rm c}_{\|{\rm a}}|_{\theta=0},$$

$$\nabla_{\|}N_{\rm a}|_{\theta=2\pi}=\Gamma^{\rm d}_{\rm a}/D^{\rm c}_{\|{\rm a}}|_{\theta=2\pi}. \tag{15}$$

The applied local constant flux boundary condition is used to simulate SMBI. It is given that the poloidal flux of molecules renders an exponential distribution. To avoid numerical instability due to a sharp gradient in the poloidal direction, the model uses an exponential profile of particle flux. Therefore, the local constant flux boundary condition is modified as follows:

$$N_{\rm m}|_{\rm edge} = N_{\rm m0}\exp\left(-\left(\theta-\theta_{1/2}\right)^2/\left(w_\theta/a\right)^2\right),\quad(\theta_0\le\theta\le\theta_1), \tag{16}$$

$$V_{x{\rm m}}|_{\rm edge} = V_{x{\rm m}0}\exp\left(-\left(\theta-\theta_{1/2}\right)^2/\left(w_\theta/a\right)^2\right),\quad(\theta_0\le\theta\le\theta_1), \tag{17}$$

where the poloidal center of the fueling source is located at $\theta_{1/2}=(\theta_0+\theta_1)/2=4.082$ rad, $w_\theta=12.56$ cm is the poloidal width of the SMB at the outermost magnetic surface, and $a=40$ cm is the minor radius of the HL-2A tokamak. In our simulation, we choose an injection velocity of $V_{x{\rm m}0}=800$ m/s and an injection density of $N_{\rm m0}=0.5N_0$. The details of these boundary conditions are explained in the literature.[25]

4. Simulation results

4.1. Effect of plasma density on penetration depth

The purpose of this paper is to study how the initial background plasma conditions affect the penetration depth of SMBI. Our simulation assessed four L-mode plasma density profiles with different gradients, while keeping the plasma temperature profile fixed. The penetration depths of the simulations during SMBI are performed until the plasma density and temperature profiles reach their steady states, which are then treated as the initial plasma profiles at $t=0$ ms. For a concise description, two symbols $N_{\rm i0}$ and $T_{\rm e0}$ are used to separately indicate the core plasma density and electron temperature at $\psi=0.65$, and $t=0$ ms. The initial densities are set to be $N_{\rm i0}=1.4N_0$, $2.2N_0$, $3.1N_0$, and $3.9N_0$, while the ion temperature profiles are fixed to 725 eV at the core (as shown in Fig. 2). The initial electron and ion temperature profiles are slightly different in their values at the core which can be ignored and they are all fixed while varying the initial density profile. The injection speed of the SMBI is set to 800 m/s, the molecule density of SMBI is set to $0.5{\rm N}_0$, and the duration of SMBI is about 1 ms. The radial transport dynamics during SMBI of the initial linear plasma density profiles mentioned above are compared as follows.

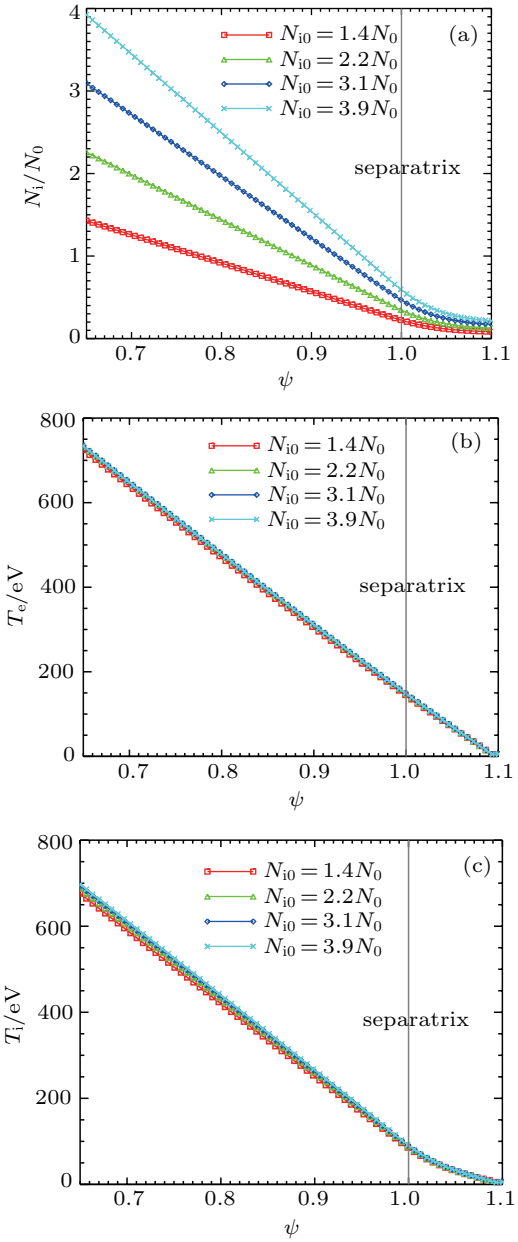


Fig. 2. (color online) (a) Radial plasma density, (b) electron temperature, and (c) ion temperature profiles at the four steady states for plasma densities of $N_{\rm i0}=1.4N_0$, $2.2N_0$, $3.1N_0$, and $3.9N_0$.

The deepest position of the propagation front of the SMB is defined as the penetration depth of the SMBI. In our simulation, the deepest penetration depth is obtained with the linear density profile having the lowest core plasma density of $N_{\rm i0}=1.4N_0$ (Fig. 3). When the core value of those linear density profiles is increased linearly from $N_{\rm i0}=1.4N_0$

to $N_{i0} = 3.9N_0$, the penetration depth decreases nonlinearly. Larger N_{i0} decreases the penetration depth. The simulated results show that the penetration depth is very low when the core density is set to $N_{i0} = 2.2N_0$ (as shown in Fig. 3), and the penetration depth continually decreases as the core plasma density increases. This behavior is caused by the stronger dissociation effect along the fueling channel of the linear density profile with a larger core density.

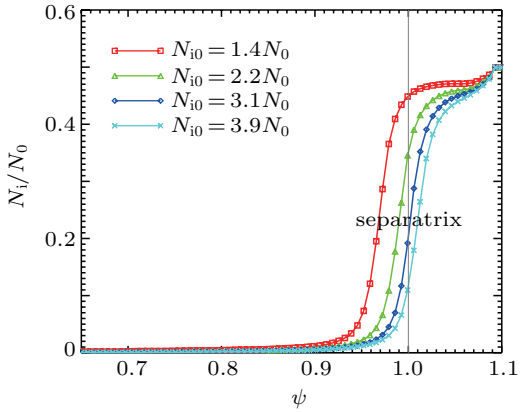


Fig. 3. (color online) Radial molecule-density profiles along the fueling path at $t = 0.4$ ms during SMBI for the initial core-plasma densities of $N_{i0} = 1.4N_0$, $2.2N_0$, $3.1N_0$, and $3.9N_0$.

We also simulate temporal evolutions of the molecular dissociation rate (shown in Fig. 4) and molecule density (shown in Fig. 5) in the radial direction. These simulations exhibit the same trend: their fronts both move quickly inwards at the early stage and move slowly outwards at the later stage because of the increase in dissociation rate. These simulations suggest that the peak of the molecular dissociation rate and the front of the SMB density will move outwards with increasing N_{i0} when the SMBI is turned on. This fact means that it is more difficult for molecules to penetrate deeper at a higher core plasma density. The analogue evolution of the molecular dissociation rate and the SMB density may block the following neutral molecules. In our simulations, the dissociation peak and the beam front for each case move inwards within 0.4 ms, then they move outwards gradually.

Figure 6 shows the simulated plasma-density profiles corresponding to the deepest propagations of different SMBs. The results suggest that the peak of the plasma density shifts outwards with increasing N_{i0}. The smallest $N_{i0} = 0.6N_0$ gives the innermost plasma density peak, while the largest $N_{i0} = 3.9N_0$ gives the outermost plasma density peak, located at the outside of the separatrix. When N_{i0} is set to $2.2N_0$, the plasma density peak is nearly located at the separatrix. Then, with increasing N_{i0}, the plasma density peak will move outwards from the separatrix. Our simulation shows that the SMBI penetration depth decreases with increasing N_{i0}. It may be caused by the neutral molecule dissociation and ionization of the SMBI beam front.

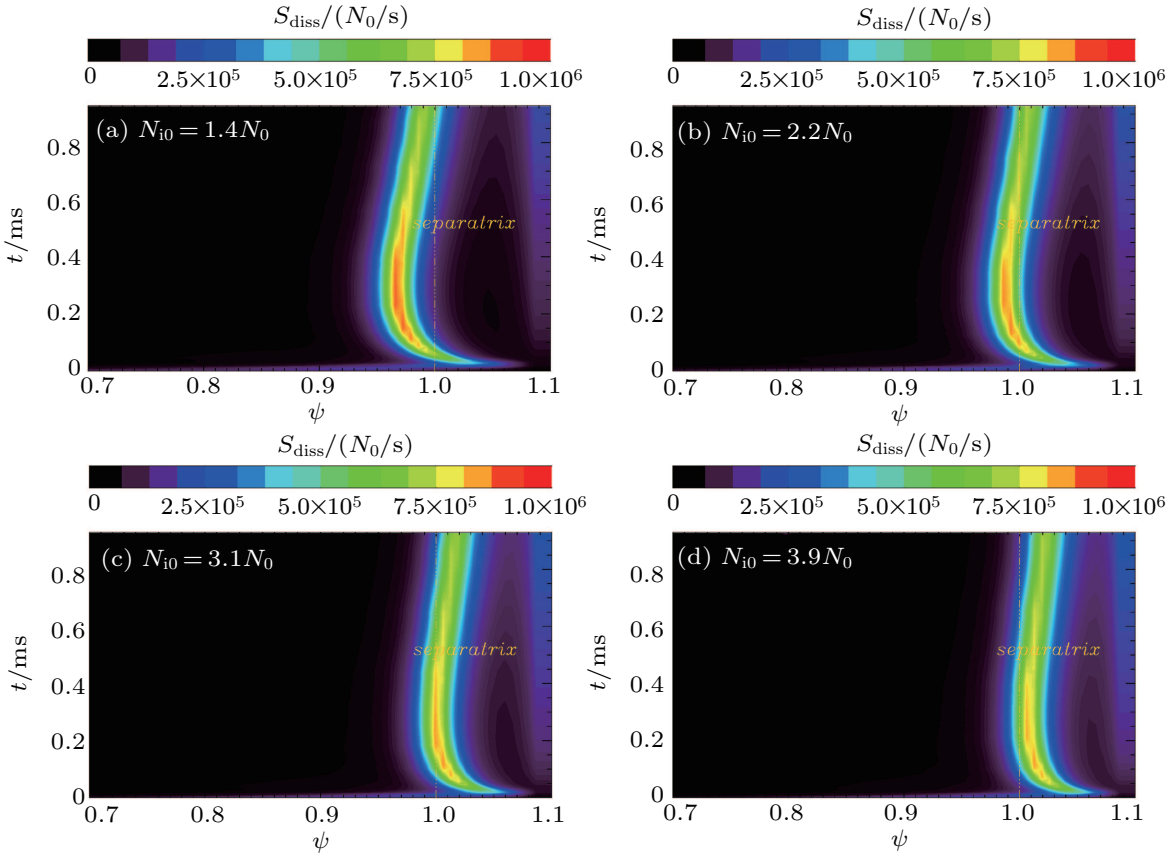


Fig. 4. (color online) The temporal and spatial evolution of neutral particle dissociation under a fixed injection flux but various initial plasma-density profiles.

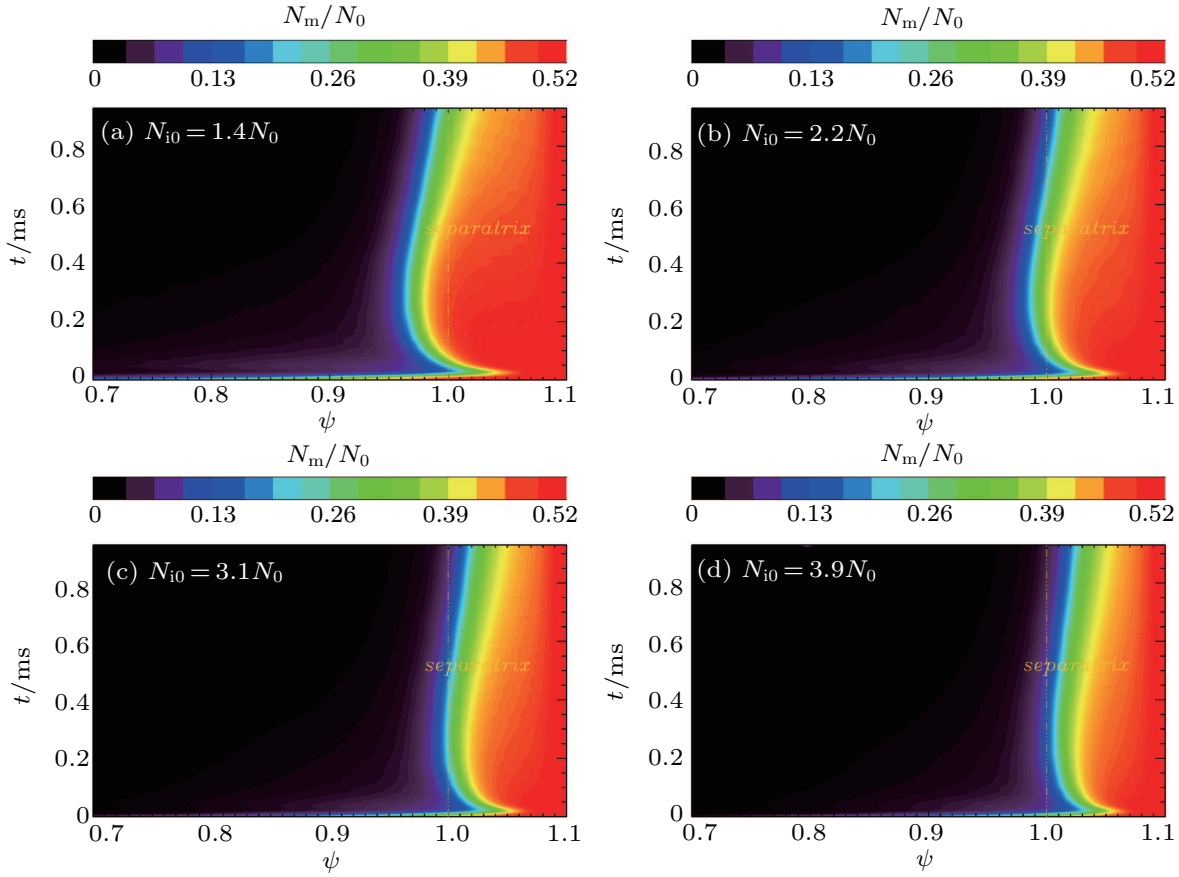


Fig. 5. (color online) The temporal and spatial evolution of molecules density under a fixed injection flux but various initial plasma-density profiles.

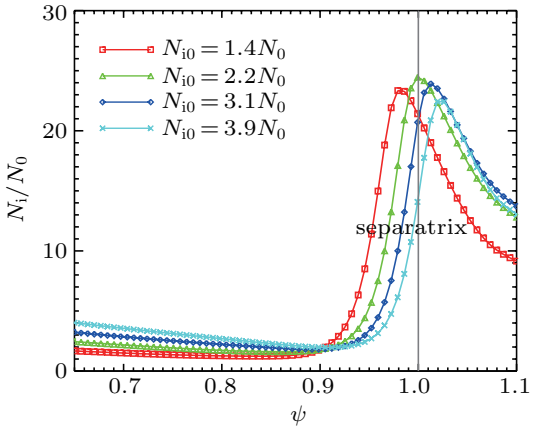


Fig. 6. (color online) Radial plasma density profiles of the four steady states corresponding to the deepest propagation of the beam front.

During SMBI, the beam is not only a particle source but also a cooling source, because the SMB temperature is much lower than the background plasma temperature. To study the cooling effect of the SMB, both the radial electron temperature profiles and the ion temperature profiles are given in Fig. 7 at $t = 0.4$ ms. The electrons and ions are much cooler within the SMB injection region than that in the inner region. This behavior occurs because the dissociation and ionization of the neutral molecules from the main SMB region consume much of the electron energy, and the ions lose their energy by ion–electron collision and recombination.

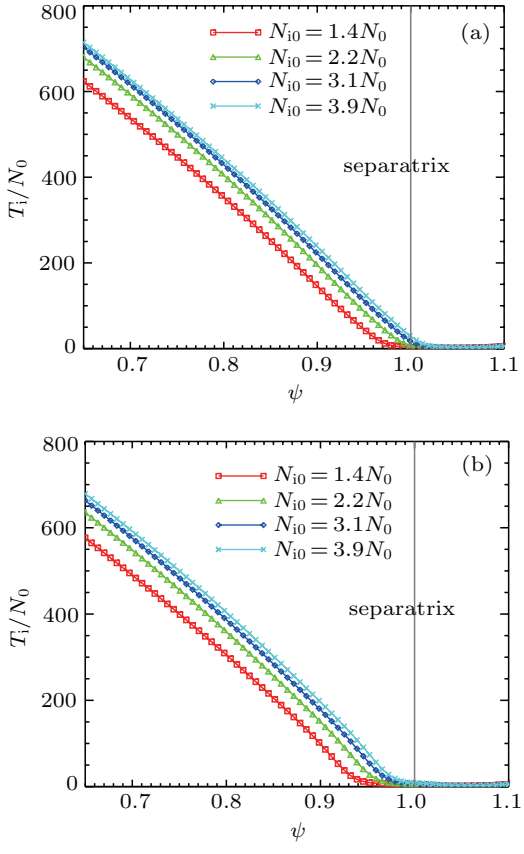


Fig. 7. (color online) Radial temperature profiles for electrons (a) and ions (b) at $t = 0.4$ ms.

4.2. Effect of plasma temperature on penetration depth

The initial plasma temperature background effects on the SMB penetration depth are also studied. With a fixed plasma-density profile of $N_{i0} = 1.4N_0$, five initial L-mode plasma temperature profiles with various gradients are used in our simulation. Both the electron temperature T_{e0} and the ion temperature T_{i0} at the core increase gradually, as shown in Fig. 8. For each case, the electron and ion temperatures at the core are slightly different. However, this difference can be ignored when studying the effects of the overall plasma temperature represented by different core electron temperatures T_{e0}.

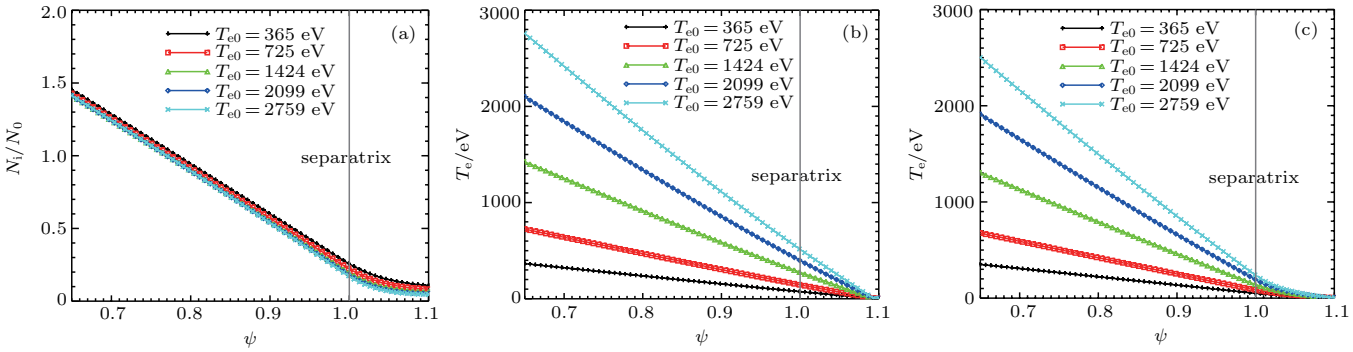


Fig. 8. (color online) (a) Radial plasma density, (b) electron temperature, and (c) ion temperature profiles at steady states for the five initial temperature profiles.

In our simulations, the deepest penetration depth is obtained by using the linear temperature profile with the lowest core plasma temperature of $T_{e0} = 365$ eV (as shown in Fig. 9). When the core plasma temperature is increased from $T_{e0} = 725$ eV to $T_{e0} = 2759$ eV, the penetration depth decreases nonlinearly in an upward convex function. Increasing T_{e0} decreases the penetration depth. It can be noticed that the penetration depth is very low when the core temperature is set to be $T_{e0} = 1424$ eV.

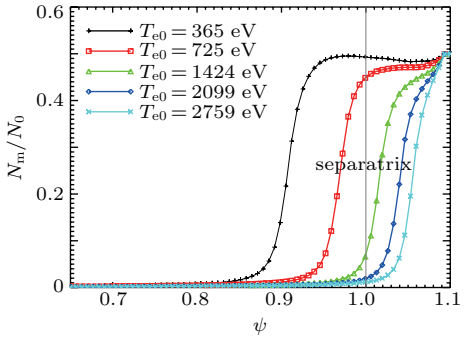


Fig. 9. (color online) Radial molecule-density profiles along the fueling path at $t = 0.4$ ms during SMBI for the five initial plasma temperature profiles.

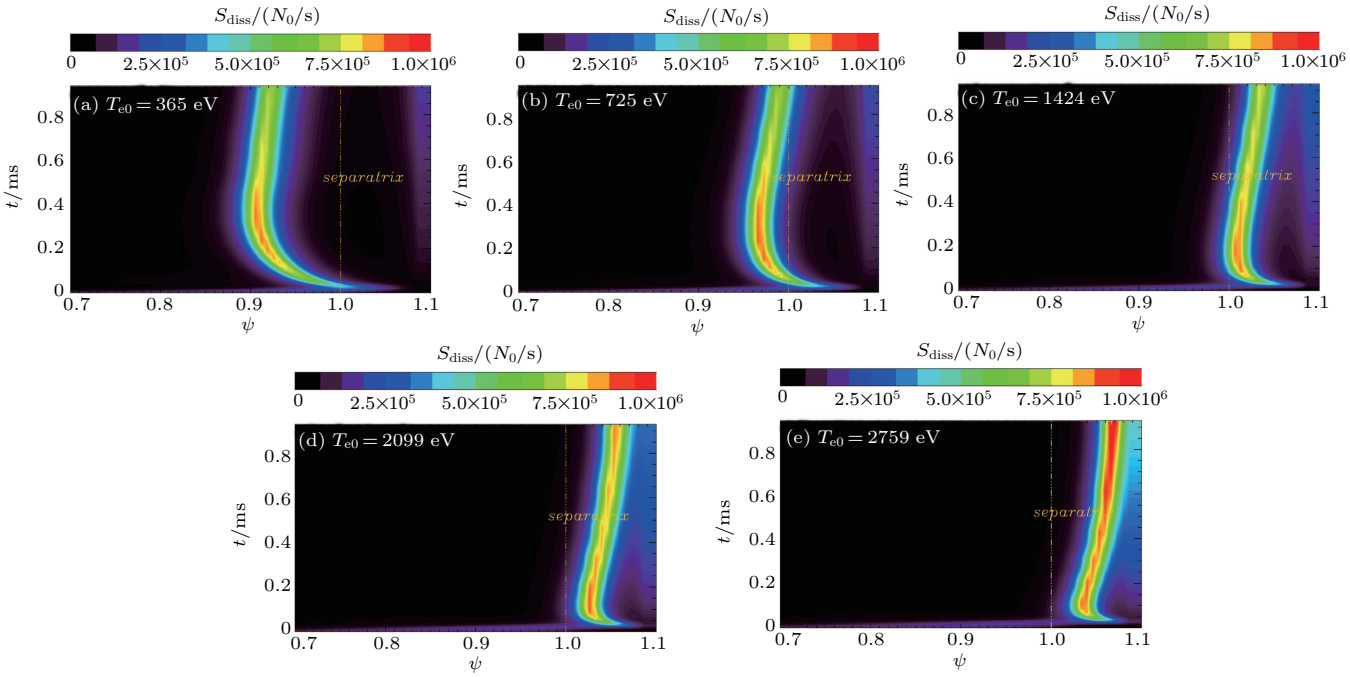


Fig. 10. (color online) The temporal and spatial evolution of neutral molecule dissociation at a constant injection flux but various initial plasma-temperature profiles.

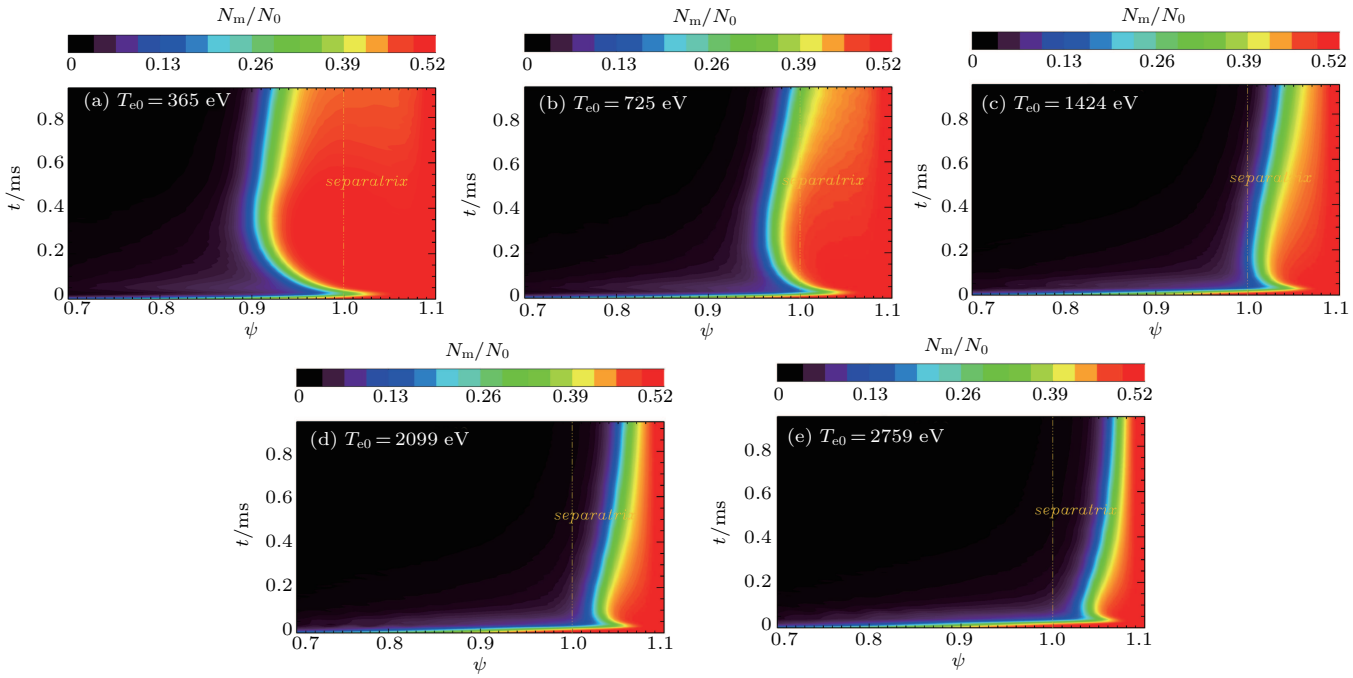


Fig. 11. (color online) The temporal and spatial evolution of molecules density at a fixed injection flux but various initial plasma-temperature profiles.

The results of varying the temperature profile but keeping the density profile (Figs. 10 and 11) are similar to those of varying the density profile but keeping the temperature profile as studied in the previous section. A high core plasma temperature produces a low SMBI penetration depth. The regions formed by the molecular dissociation rate and molecule density in the radial direction are analogous for the same SMB parameters. The molecular dissociation rate directly restricts the injection of SMB and its peak coincides with the largest gradient of molecular density, namely the propagation front. By comparing the shape of the molecular dissociation rate and the molecular density region, it is easy to find that the penetration depth and the balance time between the molecular injection rate and the overall dissociation rate will be reduced by increasing the core plasma temperature.

5. Summary and discussion

Using the *trans-neut* module of BOUT++, we have investigated how the initial plasma density and temperature profiles affect the SMBI penetration depth on which the fueling efficiency strongly depends. The radial plasma densities and temperatures are initialized to be a set of linear profiles with different core plasma densities and temperatures. The principal results and the explanations of the present simulations are summarized as follows:

(i) The penetration depth of SMB could be weakened with denser background core plasma. The injected SMB will be blocked in the SOL region when the core plasma density N_{i0} is large enough. This is due to two main reasons. One reason is that the dense background plasma makes the injected SMB molecules collide more frequently with the background plasma, and then the speed of the injected SMB front is slowed down more quickly. Therefore, the injection depth will be weakened by the dense plasma. The other reason is that the molecule dissociation rate is proportional to the plasma density as displayed in Figs. 4 and 5. Larger core plasma density N_{i0} means more molecules will be dissociated in the edge region before penetrating into the deeper region. The SMB front propagates inwards until the overall molecule dissociation rate (i.e., sink) is balanced by the SMBI rate (i.e., source). As the SMBI rate is constant, the molecule dissociation rate determines the penetration depth of the SMB. A larger core plasma density N_{i0} increases the molecule dissociation rate at the edge, decreasing the penetration depth during SMBI.

(ii) Higher core plasma temperature could also reduce the SMBI penetration depth. This behavior is similar to the case of keeping a constant initial temperature profile but varying the plasma density profile. The present simulation indicates that hot enough background plasma (i.e., $T_{e0} = 1424$ eV) blocks the injected SMB in the SOL region and makes the SMB front always located outside of the separatrix. It takes much shorter time for the SMB front moving outwards from the inside of the separatrix to the outside of the separatrix with a much higher temperature T_{e0}. The main reasons are as follows: First of all, the hotter background plasma interacts more frequently

with the injected SMB molecules, leading to larger dissociation rate, and the propagation of the beam front will be impeded, reducing the injection depth of the SMB; secondly, the neutral particles in the beam front of the injected SMB dissociate more easily in the hotter background plasma, making most of the molecules in the beam front dissociated in the edge region before propagating deeper inside. The SMB front will propagate inward when the SMBI rate overcomes the overall molecule dissociation rate. High core plasma temperature T_{e0} increases the molecule dissociation rate at the edge and decreases the penetration depth of SMBI.

In a word, both the high density and the high temperature of the background plasma make the neutral particles in the injected SMB interacted more frequently with the background species and blocked the SMB front. It is because the dissociation rate of molecules strongly depends not only on the background plasma density but also on the background plasma temperature. Both the denser density and the higher temperature of the background plasma will make the neutral particles in the beam front dissociated more easily and quickly. When more neutral injected molecules are dissociated and then ionized before propagating inwards, the plasma density at the edge region will increase and the injection depth of the SMB will decrease further in a positive feedback.

It is more difficult to penetrate inside the separatrix in high parameter plasma discharges, especially in H-mode discharges characterized by the high density and temperature in the edge region. Thus, it is necessary and urgent to find a new method to improve the SMB penetration depth and its fueling efficiency especially in the high-confinement regime. Unfortunately, the penetration depth of SMBI decreases in high-parameter plasma conditions in the present simulation, which reduces its fueling efficiency to be comparable to GP. It is not acceptable but it encourages us to improve SMBI technology urgently. To achieve the high-confinement mode in most magnetic fusion machines, such as the ITER tokamak, the fueling efficiency and fueling penetration depth must be improved, but it remains a great technical challenge to increase the penetration depth and fueling efficiency of SMBI in H-mode. Except for the effects of the background plasma conditions on the injection depth, the inherent parameters of the injected SMB (such as the injection density, injection velocity, injection width, and so on) could also affect the injection depth of the SMB. The effects of the SMB injection densities and injection velocities on the penetration depth have been done by Zhou *et al.*[14] The preliminary simulations of the effects of the injection density and injection width have been tested, which indicates that the deeper injection depth could be reached with smaller density and larger width of SMB. To find a way to increase the fueling efficiency and suggest some future experiments in the H-mode plasma conditions, more systematical and detailed simulations may be required by varying the SMBI parameters in H-mode plasma with pedestals.

Acknowledgements

The authors wish to thank Xu X Q, Dudson B D, and Umansky M V for their contributions to the BOUT++ framework.

References

[1] Sajjad S, Gao X, Ling B, Bhatti S H and Ang T 2009 *Phys. Lett. A* **373** 1133

[2] Baylor L R, Jernigan T C, Combs S K, Houlberg W A, Owen L W, Rasmussen D A, Maruyama S and Parks P B 2000 *Phys. Plasma* **7** 1878

[3] Yao L, Zhao D, Feng B, Chen C, Zhou Y, Han X, Li Y, Bucalossi J and Duan X 2010 *Plasma Sci. Technol.* **12** 529

[4] Yu D L, Chen C Y, Yao L H, Dong J Q, Feng B B, Zhou Y, Shi Z B, Zhou J, Han X Y, Zhong W L, Cui C H, Huang Y, Cao Z, Liu Yi, Yan L W, Yang Q W, Duan X R and Liu Y 2012 *Nucl. Fusion* **52** 082001

[5] Xiao W W, Zou X L, Ding X T, Yao L H, Feng B B, Song X M, Song S D, Zhou Y, Liu Z T, Yuan B S, Sun H J, Ji X Q, Gao Y D, Li Y G, Yan L W, Yang Q W, Liu Y, Dong J Q, Duan X R, Liu Y and Pan C H 2010 *Phys. Rev. Lett.* **104** 215001

[6] Xiao W W, Diamond P H, Zou X L, Dong J Q, Ding X T, Yao L H, Feng B B, Chen C Y, Zhong W L, Xu M, Yuan B S, Rhee T, Kwon J M, Shi Z B, Rao J, Lei G J, Cao J Y, Zhou J, Huang M, Yu D L, Huang Y, Zhao K J, Cui Z Y, Song X M, Gao Y D, Zhang Y P, Cheng J, Han X Y, Zhou Y, Dong Y B, Ji X Q, Yang Q W, Liu Y, Yan L W, Duan X R, Liu Y and the HL-2A Team 2012 *Nucl. Fusion* **52** 114027

[7] Sun H J, Ding X T, Yao L H, Feng B B, Liu Z T, Duan X R and Yang Q W 2010 *Plasma Phys. Control. Fusion* **52** 045003

[8] Cui X W, Cui Z Y, Feng B B, Pan Y D, Zhou H Y, Sun P, Fu B Z, Lu P, Dong Y B, Gao J M, Song S D, Yang Q W 2013 *Chin. Phys. B* **22** 125201

[9] Xiao W W, Zou X L, Ding X T, Dong J Q, Yao L H, Song S D, Liu Z T, Gao Y D, Feng B B, Song X M, Yang Q W, Yan L W, Liu Y, Duan X R, Pan C H and Liu Y 2010 *Rev. Sci. Instrum.* **81** 013506

[10] Yu D L, Chen C Y, Yao L H, Feng B B, Han X Y, Yang L M, Zhong W L, Zhou Y, Zhao K J, Huang Y, Liu Y, Yan L W, Yang Q W, Dong J Q and Duan X R 2010 *Nucl. Fusion* **50** 035009

[11] Fasoli A, Gormenzano C, Berk H L, Breizman B, Briguglio S, Darrow D S, Gorelenkov N, Heidbrink W W, Jaun A, Konovalov S V, Nazikian R, Noterdaeme J M, Sharapov S, Shinohara K, Testa D, Tobita K, Todo Y, Vlad G and Zonca F 2007 *Nucl. Fusion* **47** S264

[12] Kwon M, Oh Y K, Yang H L, Na H K, Kim Y S, Kwak J G, Kim W C, Kim J Y, Ahn JW, Bae Y S, Baek S H, Bak J G, Bang E N, Chang C S, Chang D H, Chavdarovski I, Chen Z Y, Cho K W, Cho M H, Choe W, Choi J H, Chu Y, Chung K S, Diamond P, Do H J, Eidietis N, England A C, Grisham L, Hahm T S, Hahn S H, Han W S, Hatae T, Hillis D, Hong J S, Hong S H, Hong S R, Humphrey D, Hwang Y S, Hyatt A, In Y K, Jackson G L, Jang Y B, Jeon Y M, Jeong, Jeong J I N Y, Jeong S H, Jhang H G, Jin J K, Joung M, Ju J, Kawahata K, Kim C H, Kim D H, Kim H S, Kim H S, Kim H K, Kim H T, Kim J H, Kim J C, Kim J S, Kim J S, Kim K M, Kim K M, Kim K P, Kim M K, Kim S H, Kim S S, Kim S T, Kim S W, Kim Y J, Kim Y K, Kim Y O, Ko W H, Kogi Y, Kong J D, Kubo S, Kumazawa R, Kwak S W, Kwon J M, Kwon O J, LeConte M, Lee D G, Lee D K, Lee D R, Lee D S, Lee H J, Lee J H, Lee K D, Lee K S, Lee S G, Lee S H, Lee S I, Lee S M, Lee T G, Lee W C, Lee W L, Leur J, Lim D S, Lohr J, Mase A, Mueller D, Moon K M, Mutoh T, Na Y S, Nagayama Y, Nam Y U, Namkung W, Oh B H, Oh S G, Oh S T, Park B H, Park D S, Park H, Park H T, Park J K, Park J S, Park K R, Park M K, Park S H, Park S I, Park Y M, Park Y S,

Patterson B, Sabbagh S, Saito K, Sajjad S, Sakamoto K, Seo D C, Seo S H, Seol J C, Shi Y, Song N H, Sun H J, Terzolo L, Walker M, Wang S J, Watanabe K, Welander A S, Woo H J, Woo I S, Yagi M, Yaowei Y, Yonekawa Y, Yoo K I, Yoo J W, Yoon G S, Yoon S W and the KSTAR Team 2011 *Nucl. Fusion* **51** 094006

[13] Zhou Y L, Wang Z H, Xu X Q, Li H D, Feng H and Sun W G 2015 *Phys. Plasmas* **22** 012503

[14] Zhou Y L, Wang Z H, Xu M, Wang Q, Nie L, Feng H and Sun W G 2016 *Chin. Phys. B* **25** 095201

[15] Braams B J 1996 *Contributions to Plasma Phys.* **36** 276

[16] Vold E L, Najmabadi F and Conn C R 1992 *Nucl. Fusion* **32** 1433

[17] Rognlien T D, Braams B J and Knoll D A 1996 *Contributions to Plasma Phys.* **36** 105

[18] Rognlien T D, Ryutov D D, Mattor N and Porter G D 1999 *Phys. Plasmas* **6** 1851

[19] Dudson B D, Umansky M V, Xu X Q, Snyder P B and Wilson H R 2009 *Comput. Phys. Commun.* **180** 1467

[20] Xu X Q, Umansky M V, Dudson B and Snyder R B 2008 *Commun. Comput. Phys.* **4** 949

[21] Umansky M V, Xu X Q, Dudson B, LoDestro L L and Myra J R 2009 *Comput. Phys. Commun.* **180** 887

[22] Landman I S and Janeschitz G 2007 *J. Nucl. Mater.* **363** 1061

[23] Wang Z H, Xu X Q, Xia T Y, Yu D L, Zheng G Y, Huang J, Chen S Y, Zhong W L, Shi Z B, Sun A P, Dong J Q, Xu M, Sun T T and Yao L H 2014 25*th IAEA Fusion Energy Conference* TH/P7-30

[24] Wang Y H, Guo W F, Wang Z H, Ren Q L, Sun A P, Xu M, Wang A K and Xiang N 2016 *Chin. Phys. B* **25** 106601

[25] Wang Z H, Xu X Q, Xia T Y and Rognlien T D 2014 *Nucl. Fusion* **54** 043019